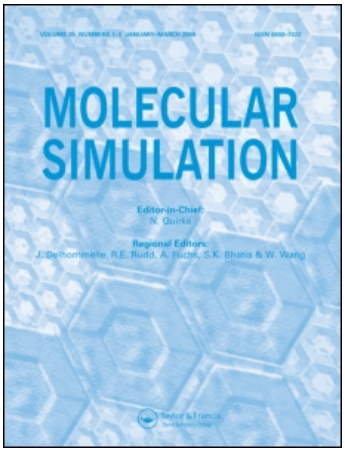

Molecular Simulation
Publication details, including instructions for authors and subscription information:
http://www.informaworld.com/smpp/title~content=t713644482

Generation of thermodynamic data for organic liquid mixtures from molecular simulations

S. Christensen[a]; G. H. Peters[b]; F. Y. Hansen[c]; J. P. O'connell[d]; J. Abildskov[a]
[a] Department of Chemical Engineering, CAPEC, DTU, Lyngby, Denmark [b] MEMPHYS-Center for Biomembrane Physics, Odense M, Denmark [c] Department of Chemistry, DTU, Lyngby, Denmark [d] Department of Chemical Engineering, University of Virginia, Charlottesville, VA, USA

To cite this Article Christensen, S. , Peters, G. H. , Hansen, F. Y. , O'connell, J. P. and Abildskov, J.(2007) 'Generation of thermodynamic data for organic liquid mixtures from molecular simulations', Molecular Simulation, 33: 4, 449 — 457
To link to this Article: DOI: 10.1080/08927020601177109
URL: http://dx.doi.org/10.1080/08927020601177109

Molecular Simulation, Vol. 33, Nos. 4–5, 15–30 April 2007, 449–457

Taylor & Francis
Taylor & Francis Group

Generation of thermodynamic data for organic liquid mixtures from molecular simulations

S. CHRISTENSEN†*, G. H. PETERS‡¶, F. Y. HANSEN‡, J. P. O'CONNELL§ and J. ABILDSKOV†

†Department of Chemical Engineering, CAPEC, DTU, Building 229, Soeltofts Plads, 2800 Kgs, Lyngby, Denmark
‡Department of Chemistry, DTU, Building 207, Kemitorvet, 2800 Kgs, Lyngby, Denmark
¶MEMPHYS-Center for Biomembrane Physics, Odense M Denmark
§Department of Chemical Engineering, University of Virginia, Charlottesville, VA 22904-4741, USA

(Received June 2006; in final form December 2006)

Fluctuation solution theory (FST) is employed to analyze results of molecular dynamics (MD) simulations of liquid mixtures. The objective is to generate parameters for macroscopic thermodynamic property models. Two benchmark systems, benzene–methyl acetate at 303.15 K and benzene–ethanol at 298.15 K, are used. MD simulations are performed in the isobaric–isothermal ensemble (*NPT*) at the respective temperatures and at a pressure of 1 atm. We use the CHARMM27 force field at different mixing ratios. We sample positions to determine the binary (between the centers-of-mass of molecules of a pair) radial distribution functions (RDFs). The RDFs are integrated to give the total correlation function integrals (TCFIs). Errors in TCFIs due to uncertainties in RDFs from simulation have been overcome by introducing a simple expression to reproduce the indirect interactions allowing reliable extrapolation to infinite distances. We compare the results of our computations with measured data on both systems studied. The results for activity coefficients agree to within experimental uncertainty.

Keywords: Fluctuation solution theory; Activity coefficients; Organic solutions; Liquids; All-atom force field; *NPT* simulations

1. Introduction

Traditionally, chemical engineering approaches to property prediction (such as group contribution methods and equations of state) have been accomplished on the basis of experimental data. Current research includes atomic-scale modeling with R&D expenditures growing relatively faster than those for experimental research. Computational chemistry is being used in concert with experimental data to establish more reliable and comprehensive property models. In this work, pair total correlation functions generated from molecular dynamic (MD) simulations are integrated for use in the fluctuation solution theory (FST) of Kirkwood and Buff [1] that yields derivatives of the chemical potential, or equivalently, activity coefficients and of density. Two systems have been analyzed: benzene and ethanol at 298.15 K which is moderately nonideal and benzene with methyl acetate at 303.15 K which is only slightly nonideal.

2. Fluctuation solution theory

FST describes the connection between the local composition at microscopic level and the macroscopic properties of a fluid [1]. The key quantity is the total correlation function integral (TCFI), H_{ij}, given by [2]:

$$H_{ij} = 4\pi\rho\int_0^\infty r^2\left(g_{ij}^{\mu VT}(r) - 1\right)\mathrm{d}r \qquad (1)$$

where ρ is the molecular density of the system which is the average value from *NPT* simulations. r is the center-of-mass to center-of-mass distance between molecules of type i and j and $g_{ij}^{\mu VT}(r)$ is the radial distribution function (RDF) in the grand canonical ensemble. For angle dependent intermolecular forces, the integration includes all orientations. Also, the results do not depend on pairwise additivity of the intermolecular interactions. The macroscopic partial molar volumes, $\bar{V}_1$, isothermal

*Corresponding author. Email: ja@kt.dtu.dk

Molecular Simulation
ISSN 0892-7022 print/ISSN 1029-0435 online © 2007 Taylor & Francis
http://www.tandf.co.uk/journals
DOI: 10.1080/08927020601177109

compressibility, κ_T and activity coefficient derivatives, $(\partial \ln \gamma_1/\partial x_1)_{T,P}$ are related to the TCFIs by:

$$\rho\kappa_T kT = \frac{1 + x_1H_{11} + x_2H_{22} + x_1x_2\left(H_{11}H_{22} - H_{12}^2\right)}{1 + x_1x_2\Delta H} \tag{2}$$

$$\rho\bar{V}_1 = \frac{1 + x_2(H_{22} - H_{12})}{1 + x_1x_2\Delta H} \tag{3}$$

$$\left(\frac{\partial \ln \gamma_1}{\partial x_1}\right)_{T,P} = \frac{-x_2\Delta H}{1 + x_1x_2\Delta H} \tag{4}$$

$$\Delta H = H_{11} + H_{22} - 2H_{12} \tag{5}$$

where x_i is the mole fraction of i. Interchanging subscripts gives the relationships for component 2. These equations show that FST provides a direct relationship between RDFs obtained from simulations and measurable thermodynamic properties. FST has been used by various researchers to investigate the properties of liquid mixtures. Some studies extract the appropriate FST integrals from experimental data [3–5] while others have determined FST integrals from computer simulations [6].

3. Reverse approach; TCFIs from thermodynamic models

Since properties can be expressed in terms of TCFIs, a reverse procedure can be used to obtain TCFI values from property data [3–5]. In particular, a data bank of TCFIs for binary mixtures were generated using such a reverse approach [5]. The experimental data were regressed using Redlich/Kister-like polynomials [7] for densities, ρ, and partial molar volumes, $\bar{V}_i$, the Huang-O'Connell [8] model for isothermal compressibilities, κ_T, and the NRTL, modified Margules (mM) or Wilson G^E-models from phase equlibria used to calculate activity coefficient derivatives, $(\partial \ln \gamma_1/\partial x_1)_{T,P}$ [9]. The route to TCFIs was via integrals of the direct correlation function of Ornstein and Zernike, C_{ij},

$$(1 - C_{11}) = \frac{\rho\bar{V}_1^2}{\kappa_T RT} + x_2\left(\frac{\partial \ln \gamma_1}{\partial x_1}\right)_{T,P} \tag{6}$$

$$(1 - C_{12}) = \frac{\rho\bar{V}_1\bar{V}_2}{\kappa_T RT} - x_1\left(\frac{\partial \ln \gamma_1}{\partial x_1}\right)_{T,P} \tag{7}$$

$$(1 - C_{22}) = \frac{\rho\bar{V}_2^2}{\kappa_T RT} + x_1\left(\frac{\partial \ln \gamma_2}{\partial x_2}\right)_{T,P} \tag{8}$$

which were then converted to TCFIs by an integrated form of the Ornstein–Zernike equation [2],

$$H_{11} = \left(\frac{1 - x_2C_{22}}{D} - 1\right)\frac{1}{x_1} = \frac{C_{11} - x_2\left(C_{11}C_{22} - C_{12}^2\right)}{D} \tag{9}$$

$$H_{12} = \frac{C_{12}}{D} \tag{10}$$

$$H_{22} = \left(\frac{1 - x_1C_{11}}{D} - 1\right)\frac{1}{x_2} = \frac{C_{22} - x_1\left(C_{11}C_{22} - C_{12}^2\right)}{D} \tag{11}$$

$$D = (1 - x_1C_{11})(1 - x_2C_{22}) - x_1x_2C_{12}^2 \tag{12}$$

4. Thermodynamic models from TCFIs

There are several options for comparing simulation and experiment. We compare the TCFIs found from MD simulations with TCFIs found from the above procedure. We also compare activity coefficient derivatives from fitting the mM model [9]

$$\frac{G^E}{RTx_1x_2} = A_{21}x_1 + A_{12}x_2 - \frac{\alpha_{12}\alpha_{21}x_1x_2}{\alpha_{12}x_1 + \alpha_{21}x_2 + \eta x_1x_2} \tag{13}$$

to experimental data, with derivatives from simulation using equation (4). This formulation uses the Lewis/Randall pure-component standard state. Note that the original treatment [1] used the Henry's law standard state,whereas a later development [2] allowed a choice of standard state. A likely advantage of building activity coefficient models from derivatives is that the ultimate properties are less sensitive to errors in the basic model. The model parameters for the simulations were determined by minimizing the objective function

$$\mathrm{SS} = \sum\left[\left(\frac{\partial \ln \gamma_1}{\partial x_1}\right)_{\mathrm{MD}} - \left(\frac{\partial \ln \gamma_1}{\partial x_1}\right)_{\mathrm{mM}}\right]^2 \tag{14}$$

where subscript MD denotes results obtained from FST analysis of MD results. mM denotes derivatives calculated by the mM model using the adjustable parameters. Following the approach given in [9], the initial regression was for the two-parameters, A_{12} and A_{21}. Then a four-parameter regression followed by adjusting A_{12}, A_{21}, α_{12} and α_{21}. If SS decreased significantly, as it typically did, a final five-parameter regression was made adjusting also η. If again SS was reduced significantly, as sometimes occurred, the five-parameter set was selected to describe the system. Using parameters obtained from this procedure, it is possible to calculate activity coefficient data covering the complete composition range of complex systems [9]. In this work, experimental derivatives for ethanol with benzene [5] and methyl acetate with benzene [10] were compared with those generated from simulations.

5. Simulation details

Previous simulation work suggests that FST analysis of simulation results can provide quantitative information concerning the thermodynamics of solutions [6,11].

We use the equivalence of ensembles and have determined TCFIs from the quantity:

$$H_{ij} = 4\pi\rho\int_0^{r_{\max}} r^2\left(g_{ij}^{NPT}(r) - 1\right)\mathrm{d}r \qquad (15)$$

using the isobaric–isothermal ensemble (*NPT*) rather than the grand canonical ensemble (see equation (1)) since it is more convenient in an MD simulation. We used NAMD [12] for MD simulations. Periodic boundary conditions were imposed and the time step used in the integration was 1 fs. A cut-off distance of 12 A was applied together with a switching function at 10 A. The particle-mesh-Ewald (PME) algorithm was used to calculate long-range electrostatic forces [12]. The starting configuration was built from the equilibrium configuration of a single molecule. The simulation box was divided into a simple grid and the molecule templates were inserted at the grid points in accordance with the desired composition. We used 512 molecules for simulating ethanol/benzene and 1000 for methyl acetate/benzene. Two steps were used for equilibrating the system. Firstly, the system was relaxed by a steepest descent method to eliminate atomic overlaps in the initial setup of the system. This process was terminated when the system potential energy became essentially constant. Secondly, the *NPT* simulations (pressure of 1 atm and a temperature equal to the experimental value) were started and run for 500 ps. The criterion for terminating at this stage was that there was negligible variation in the radial pair distribution functions. Then the production period was started. Its length varied somewhat with the composition. In most cases, periods of 15–18 ns were used, sampling positions at intervals of 500 fs. Statistics were obtained by dividing the trajectories into three blocks.

5.1 Force field

The all-atom CHARMM27 force field was used in the simulations [13,14]. The parameters used are listed in tables 1–6. The force field is characterized by harmonic

Table 1. Atom descriptions and charges taken from the CHARMM27 force field.

Atom	*Description*	*q*
Benzene		
CA	Aromatic carbon	−0.115
HP	Aromatic hydrogen	0.115
Ethanol		
H	Alcohol hydrogen	0.430
OH1	Alcohol oxygen	−0.660
CT2	Methylene carbon	0.050
CT3	Methyl carbon	−0.270
HA	Alkane hydrogen	0.09
Methyl acetate		
CT3	Methyl carbon (acetate)	−0.17
CD	Acetate carbon	0.63
OB	Acetate oxygen (double bond)	−0.52
OS	Acetate oxygen (single bond)	−0.34
CT3	Methyl carbon (single oxygen bond)	−0.14
HA	Alkane hydrogen	0.09

Table 2. Bond vibration parameters taken from the CHARMM27 force field.

Bond	K_b *(kcal/mole/A*^{2}*)*	b_0 *(A)*
CA–CA	305.0	1.375
CA–HP	340.0	1.080
OH1–H	545.0	0.960
CT2–OH1	428.0	1.420
CT2–CT3	222.5	1.528
CT2–HA	309.0	1.111
CT3–HA	322.0	1.111
CT3–CD	200.0	1.522
OB–CD	750.0	1.220
OS–CD	150.0	1.334
OS–CT3	340.0	1.430

Table 3. Bond angle and UB parameters taken from the CHARMM27 force field. (···) Indicate that no UB terms is applied for this atomic pair.

Angle	K_q *(kcal/mole rad*^{2}*)*	q_0	K_{UB} *(kcal/mole A*^{2}*)*	S_0 *(A)*
CA–CA–CA	40.0	120.00	35.00	2.4162
CA–CA–HP	30.0	120.00	22.00	2.1525
H–OH1–CT2	57.5	106.00	···	···
OH1–CT2–CT3	75.7	110.10	···	···
OH1–CT2–HA	45.9	108.89	···	···
CT2–CT3–HA	34.6	110.10	22.53	2.1790
CT3–CT2–HA	34.6	110.10	22.53	2.1790
HA–CT2–HA	35.5	109.00	5.40	1.8020
HA–CT3–HA	35.5	108.40	5.40	1.8020
CT3–OS–CD	40.0	109.60	30.00	2.2651
HA–CT3–CD	33.0	109.50	30.00	2.1630
OB–CD–CT3	70.0	125.00	20.00	2.4420
OS–CD–CT3	55.0	109.00	20.00	2.3260
OS–CD–OB	90.0	125.90	160.00	2.2576
OS–CT3–HA	60.0	109.50	···	···

Table 4. Dihedral angle parameters taken from the CHARMM27 force field. *X* can be any atom.

Dihedral angle	K_χ *(kcal/mole)*	*n*	δ
CA–CA–CA–CA	3.100	2	180.00
CA–CA–CA–HP	4.200	2	180.00
HP–CA–HP–CA	2.400	2	180.00
OH1–CT2–CT3–HA	0.160	3	0.00
H–OH1–CT2–CT3	1.300	1	0.00
H–OH1–CT2–HA	0.140	3	0.00
HA–CT2–CT3–HA	0.160	3	0.00
OB–CD–OS–CT3	0.965	1	180.00
OB–CD–OS–CT3	3.850	2	180.00
X–CD–OS–X	2.050	2	180.00
X–CT3–CD–X	0.000	6	180.00
X–CT3–OS–X	−0.100	3	0.00

Table 5. Improper dihedral angle parameters taken from the CHARMM27 force field. *X* can be any atom.

Dihedral angle	K_φ (kcal/mole)	φ_0
CD–X–X–OB	100.00	0.00

Table 6. Lennard–Jones parameters taken from the CHARMM27 force field. ··· Indicate that no special parameters are used for 1–4 interactions.

Atom	ϵ(kcal/mole)	$R_{min}/2$ (A)	ϵ^{1-4} (kcal/mole)	$R^{1-4}_{\min}/2$ (A)
CA	−0.0700	1.9924	···	···
HP	−0.0300	1.3582	···	···
H	−0.0460	0.2245	···	···
OH1	−0.1521	1.7700	···	···
CT2	−0.0550	2.1750	−0.0100	1.9000
CT3	−0.0800	2.0600	−0.0100	1.9000
HA	−0.0220	1.3200	···	···
CD	−0.0700	2.0000	···	···
OB	−0.1200	1.7000	−0.1200	1.4000
OS	−0.1521	1.7700	···	···

potentials for flexible bonds, a Urey–Bradley (UB) term for 1–3 interactions and a Lennard–Jones term for 1–4 interactions and other non-bonded interactions in general. The UB term was applied in different ways, so table 3 has dots (···) to mark the angles where the UB term is not applied. In special cases, a modified parameter set was used for 1–4 interactions [13], such as the alkane carbon atoms in ethanol shown in [table 6]. For others, the same Lennard–Jones parameters are applied both to 1–4 and non-bonded interactions (...in table 6). Coulombic forces are included using charges positioned at the centers of mass of the atoms where interactions are included for atoms separated by three or more bonds. The general form of the potential is given by:

$$U(R) = \sum_{\text{bonds}} K_b(b-b_0)^2 + \sum_{\text{angles}} K_\theta(\theta-\theta_0)^2 + \sum_{\text{UB}} K_{\text{UB}}(S-S_0)^2 + \sum_{\text{dihedrals}} K_\chi(1+\cos(n\chi-\delta)) + \sum_{\text{impropers}} K_\varphi(\varphi-\varphi_0)^2 + \sum_{\text{nonbond}} \left(\epsilon_{ij}\left[\left(\frac{R_{\min,ij}}{r_{ij}}\right)^{12} - 2\left(\frac{R_{\min,ij}}{r_{ij}}\right)^{6} \right] + \frac{q_i q_j}{\epsilon_1 r_{ij}} \right) \tag{16}$$

where K_b, K_{UB}, K_θ, K_χ and K_φ are the bond, UB, angle, dihedral angle and improper dihedral angle force constants, respectively; b, S, θ, χ and φ are the bond length, UB 1,3-distance, bond angle, dihedral angle and improper torsion angle, respectively and the subscript zero represents equilibrium values for the individual terms. ϵ_{ij} is the Lennard–Jones well depth and $R_{\min,ij}$ is the distance at the minimum of the Lennard–Jones potential. The unlike Lennard–Jones parameters are calculated with Lorentz–Berthelot combining rules. q_i is the atomic partial charge, ϵ_1 is the effective dielectric constant and r_{ij} is the distance between atoms i and j. The dielectric constant is set to one in all calculations, corresponding to the permittivity of vacuum [15].

5.2 Integration of radial distribution function

The integral in equation (15), has a finite upper limit, $r_{\max}$. The treatment of this can be complicated by the limited range, set by the simulation box, for which we may simulate $g_{ij}(r)$ and the slow convergence of $g_{ij}(r)$ toward the asymptotic value of unity. The maximum distance, $r_{\max}$, equals half the side length of the simulation box, L_{box}. Theoretically, $g_{ij}(r) - 1$ goes to zero when r goes to infinity. However, because the integral is evaluated numerically, convergence requires that $g_{ij}(r) - 1$ goes faster to zero than r^2 goes to infinity. If not, the integral diverges. Occasionally, this can create problems. For example, convergence of $g_{ij}(r)$ may not be attained at $r = r_{\max}$. The deviation of $g_{ij}(r)$ from unity may be about 0.1–0.2% or less. Yet, this magnifies in the TCFI because of the r^2 factor in the integrand, as illustrated in figure 1 for the ethanol–ethanol RDF.

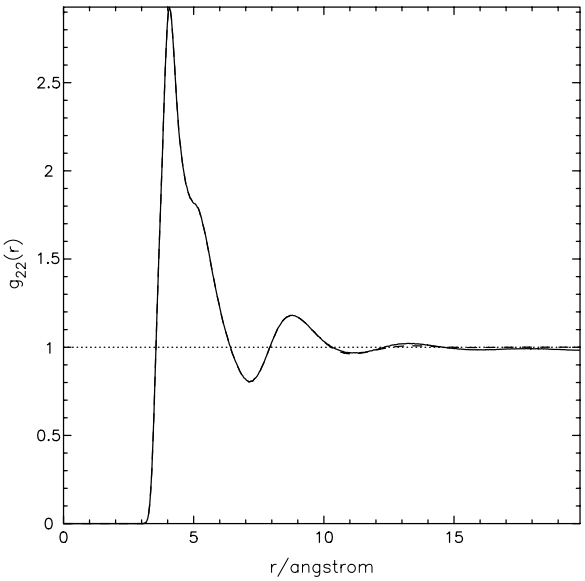

(a) $g_{22}(r)$ at $x_1 = 0.5$

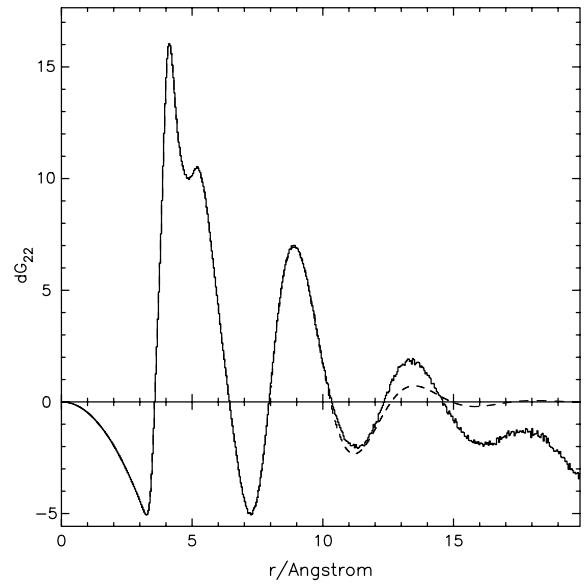

(b) Integrand, dG_{22} at $x_1 = 0.5$

Figure 1. Effect of divergence of $g_{ij}(r)$ at longer distances. $x_1 = 0.5$, where 1: benzene and 2: ethanol. Solid line represents method 1. Dashed line is a fit using equation (17) with method 3.

The solid line in figure 1(a) is $g_{22}(r)$ which visually does not deviate from unity near r_{max}. However, the divergence is clearly seen on figure 1(b) starting at $r \approx 15$ A where a local maximum in the integrand, dG_{22}, has a negative value. To overcome these difficulties, three levels of approximation have been considered.

The first approach (method 1) is simply to stop integration when a sub unity maximum or above unity minimum in $g_{ij}(r)$ is encountered. This gives an approximate H_{ij} value. Method 2 is to increase the size of the system simulated and redo the simulations. Literature provides examples [6] of this, although it increases the simulation time significantly. A method 3 uses a simple expression to reproduce the indirect interaction part of $g_{ij}(r)$ which approaches unity faster than r^2 goes to infinity. The expression used is:

$$g_{ij}^{\text{indirect}}(r) = 1 + a\exp(b(r-c))\sin(d(r-e)) \qquad (17)$$

The five-parameters are determined by regression where the objective is to reproduce $g_{ij}(r)$ from the third unity, r_{u3}, until either r_{max} or the distance where $g_{ij}(r)$ diverges. An example is shown in figure 1 where the dashed curve is the result of such a regression. When applying the expression it is possible to integrate the g_{ij}^{indirect} until r_{max}. But it is also possible to extrapolate using the expression from r_{max} to radius, r_{nc}, where there is no longer any contribution to the TCFI. The contribution to H_{ij} from integration from r_{max} to r_{nc} is viewed as a long distance correction term, H_{ij}^{ld}, and practically this approach enables integration from zero to infinity. The final form for TCFIs has three contributions. The direct interaction part of the RDF is integrated numerically giving first contribution, H_{ij}^{direct}. The second contribution is the integration of equation (17) from the start of the indirect interaction part of the RDF (third unity) to the maximum distance determined by the box size, H_{ij}^{box} and the final term is the long distance correction term, H_{ij}^{ld}.

$$H_{ij} = H_{ij}^{\text{direct}} + H_{ij}^{\text{box}} + H_{ij}^{\text{ld}} \qquad (18)$$

The statistical uncertainty of the direct interaction part of the RDFs was negligbile. It was small for the first portion of the indirect part, but could be significant at longer distances. Fortunately the contribution of H_{ij}^{ld} to H_{ij} is numerically the smallest of all three terms. In practice, if method 3 does not give reasonable results due to the shape of $g_{ij}(r)$, methods 1 or 2 should be used.

6. Results

Our focus is on activity coefficients, so we have compared results of the ethanol–benzene simulations with results [5] obtained for the same system using the reverse approach described above. Figure 2 shows that the TCFIs generated by the reverse approach using NRTL, mM and Wilson G^E-models vary significantly, although the trends with composition are similar. The large first peak in the ethanol–ethanol RDF (figure 1(a)) results from ethanol self-association. This is reflected in the large positive H_{22} of figure 2(c) which should be compared with the much smaller values for the benzene–benzene (H_{11}) and benzene–ethanol (H_{12}) TCFI. These qualitative features of our results are confirmed by the results of Wooley and O'Connell [5].

Now *NPT* simulations also yield values for the system volume/density at the specified *T*, *P* and composition. We compare our simulation pure component molar volumes obtained from simulations with measured values in table 7. Although the agreement is not quantitative, the values are reasonably close and we concluded that no refinements of the force fields were necessary.

The equivalence of ensembles is only true for infinitely large systems. It is also true for smaller systems, but the fluctuations are larger for the smaller systems, and the systems may be so small that a thermodynamical description is meaningless. We are not at that limit here. Table 8 compares TCFIs obtained from simulations of 512 and 1000 molecules of the benzene/ethanol binary at $x_1 = 0.9$. The uncertainties are—as expected—smaller with 1000 molecules, but the final results do not differ significantly.

We wanted to evaluate the consequences of the alternative integration treatments, especially method 1 vs. method 3. Figure 3 compares the results of calculating TCFIs based on method 1 where the integral is truncated with method 3 where equation (17) is used for the long-range contribution. While this indicates that both sets of TCFIs give good results, comparisons using plots like figure 2, consistently showed better agreement with the reverse approach results when method 3 was employed. On the other hand, the principal quantity for activity coefficient derivatives is not the individual TCFIs but their difference, ΔH of equation (5). Therefore, although the individual TCFIs may vary significantly, the differences can be similar, yielding similar activity coefficient derivatives. This suggests that method 1 may be adequate for thermodynamic property purposes even if it is inferior to method 3 for statistical mechanical properties. Our results for the methyl acetate–benzene binary at 303.15 K are given in figure 4. In this case, the consistency of the results using method 3 with the mM correlation is clear. At this time, we know of no reverse approach results for the benzene–methyl acetate binary, so the accuracy of either approach for statistical mechanical properties is unknown.

7. Conclusion

FST has been applied to compare thermodynamic derivative properties from molecular dynamics simulation

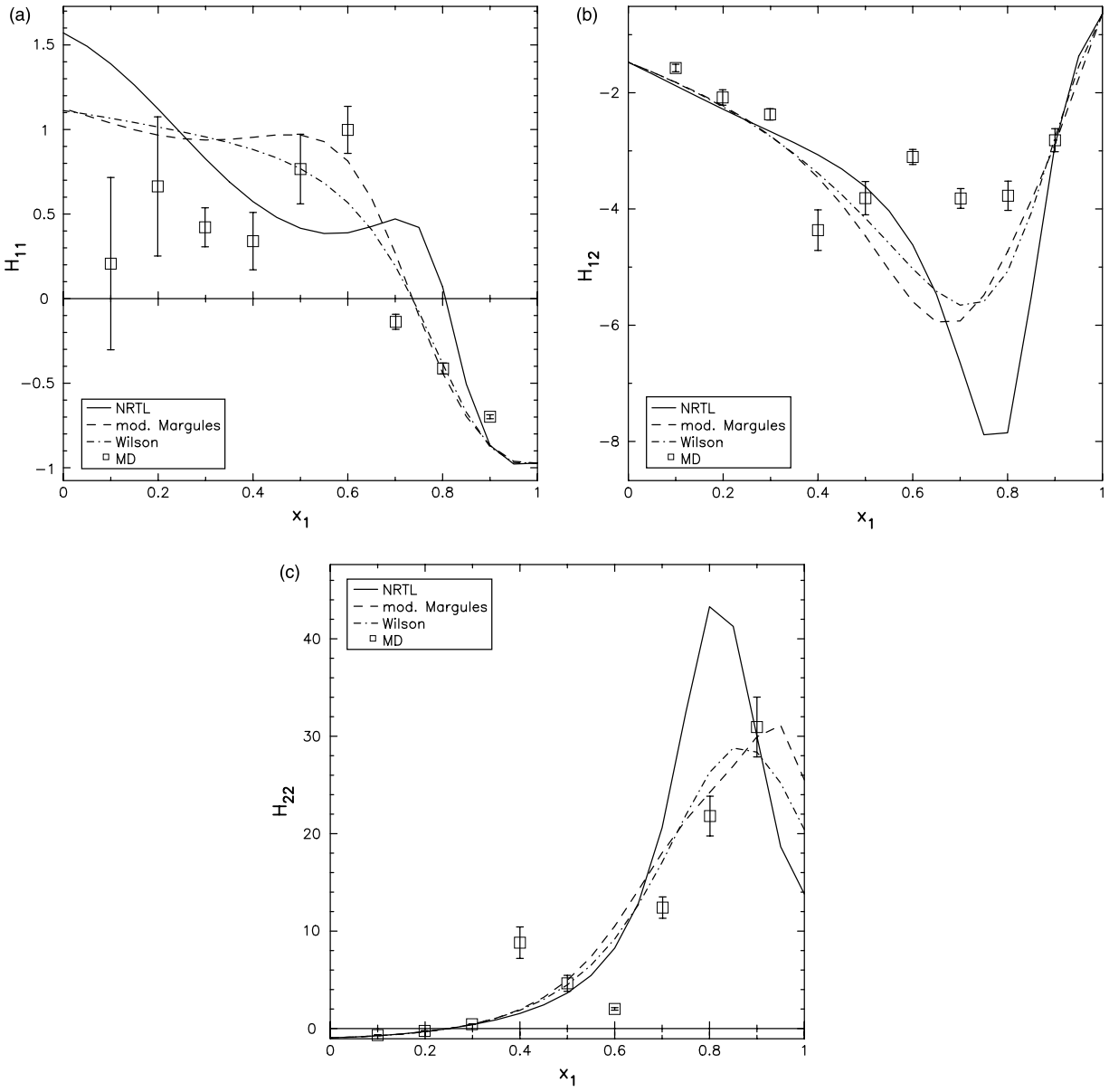

Figure 2. TCFIs for (a) benzene/benzene, H_{11}, (b) benzene/ethanol, H_{12}, (c) ethanol/ethanol, H_{22}, at 298.15 K and 1 atm. TCFIs from method 3. Lines are generated using the reverse approach of Wooley and O'Connell [5] with G^E-models.

to those from experiment. Methods have been compared to obtain converged values of the molecular integrals involving RDFs. The best results are obtained when combining numerical integration of short-range RDF with a convergent analytical correlation of the long-range behavior. The results are good reproductions of activity coefficient derivatives from measured phase equilibria at all compositions and individual TCFIs in good agreement

Table 7. Comparing pure compound molar volumes for benzene, ethanol and methyl acetate at different temperatures.

Compound	V_m^{exp} (cm^3/mol)	V_m^{MD} (cm^3/mol)	*Relative error %*
Benzene–ethanol at 298.15 K			
Benzene	89.502	92.08 ± 0.72	2.9
Ethanol	58.516	59.56 ± 0.57	1.8
Benzene–methyl acetate at 303.15 K			
Benzene	89.961	92.82 ± 0.54	3.2
Methyl acetate	80.442	81.75 ± 0.45	1.6

Table 8. Comparing TCFIs for benzene–ethanol system at $x_B = 0.9$ using methods 1 and 3 for integration in two setups with 512 and 1000 molecules, respectively.

Number of molecules	*Integration method*	H_{11}	H_{12}	H_{22}
512	1	-0.595 ± 0.011	-2.29 ± 0.18	30.9 ± 3.8
	3	-0.689 ± 0.016	-2.78 ± 0.23	⋯
1000	1	-0.6631 ± 0.0091	-2.317 ± 0.0081	29.8 ± 1.1
	3	-0.8333 ± 0.0059	-2.851 ± 0.043	⋯

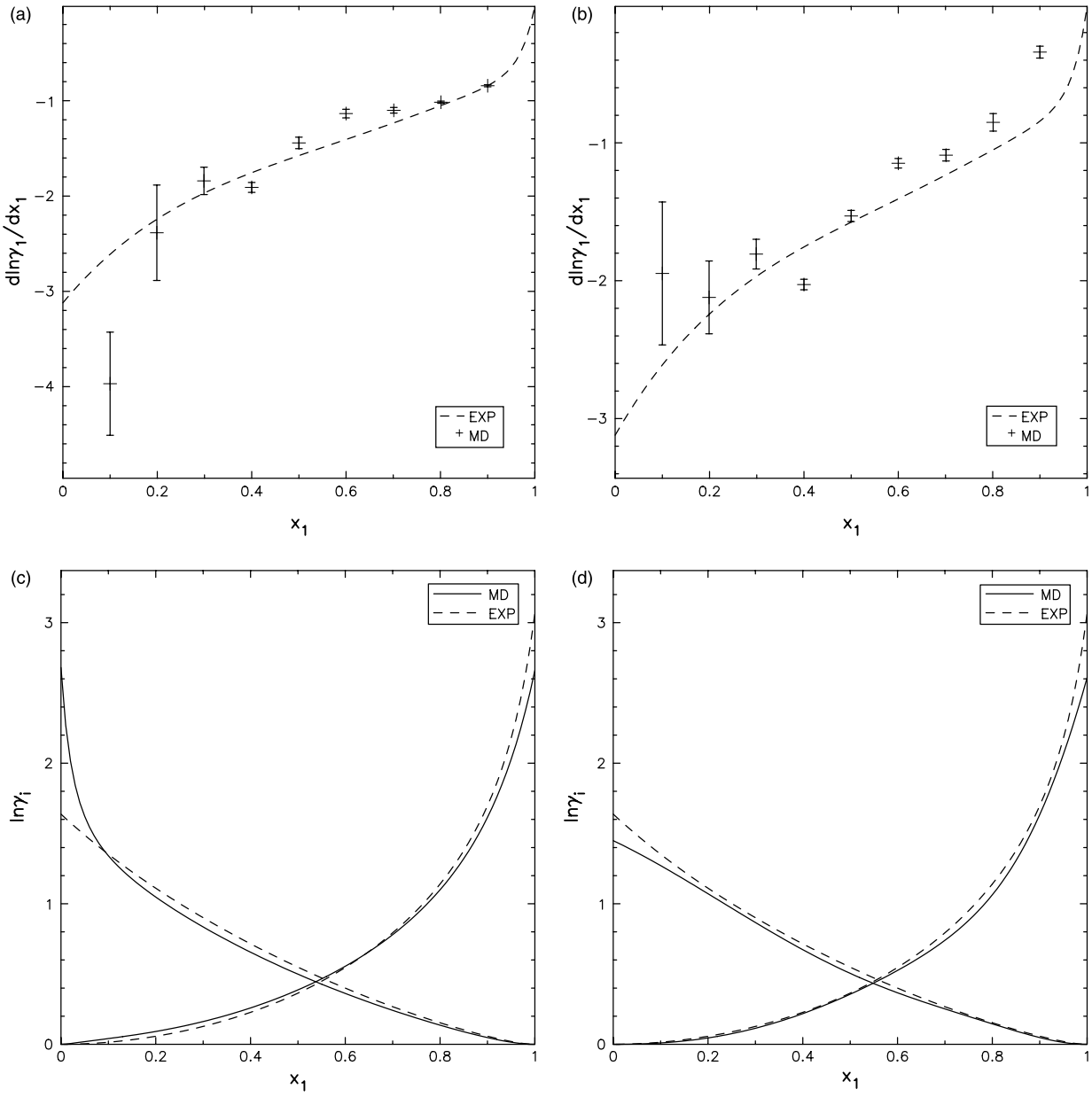

Figure 3. Benzene(1)–ethanol(2) at 298.15 K and 1 atm. Comparing results of MD results with mM correlation. Figures (a) and (c) use the TCFIs found using method 1. Figures (b) and (d) use the TCFIs found using method 3. Crosses and solid lines are results from MD simulations. Dashed lines are generated by mM where the parameters have been determined using experimental data.

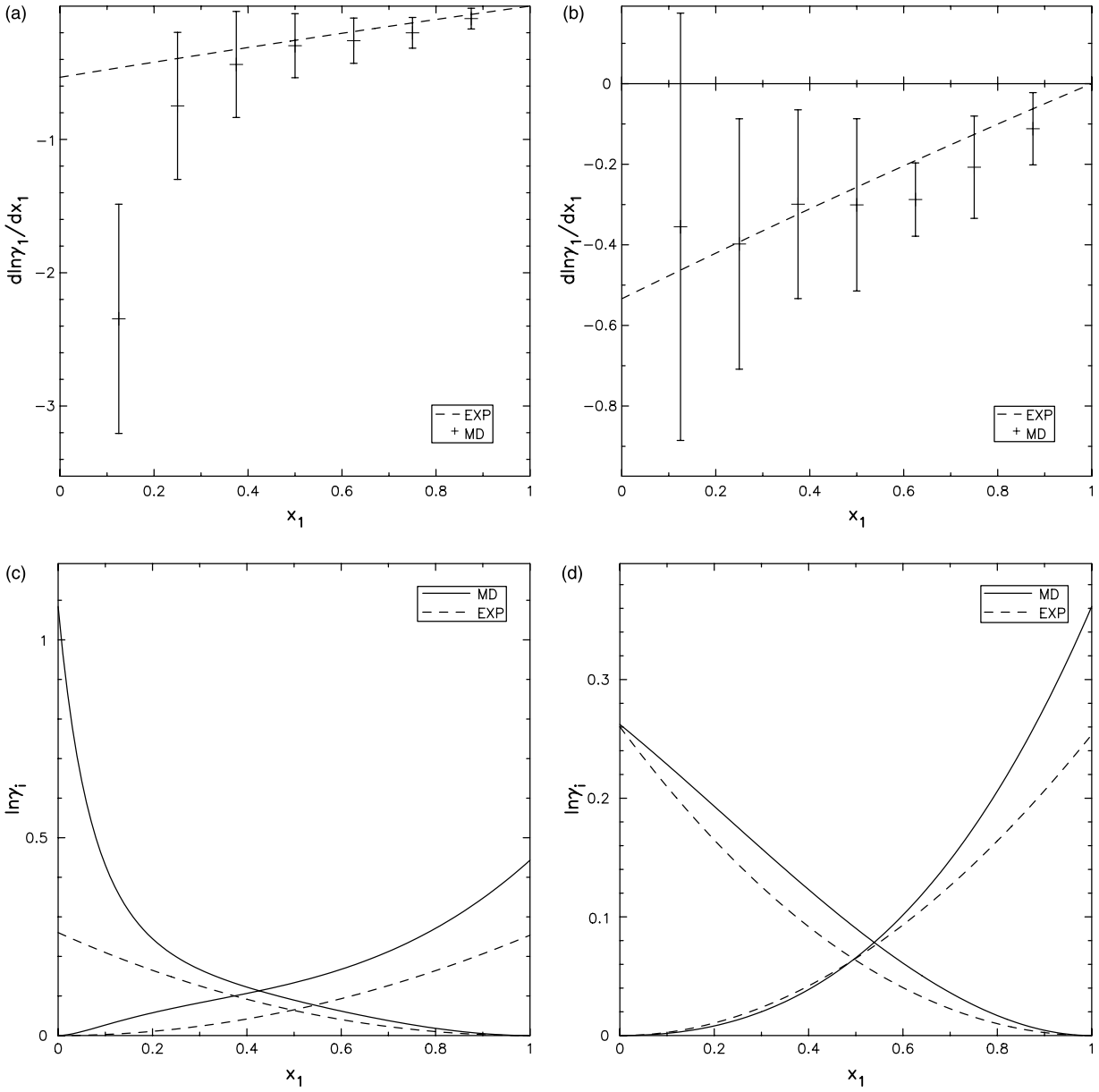

Figure 4. Benzene (1)–methyl acetate (2) at 303.15 K and 1 atm. Comparing results of MD results with mM correlation. Figures (a) and (c) use the TCFIs found using method 1. Figures (b) and (d) use the TCFIs found using method 3. Crosses and solid lines are results from MD simulations. Dashed lines are generated by mM where the parameters have been determined using experimental data.

with those obtained from literature data [5]. This approach represents an alternative development and characterization of engineering equations of state or excess Gibbs energy models for liquid mixtures that may be of value in both fundamental research and in applications to complex systems.

Acknowledgements

The authors gratefully acknowledge access to the Danish Center for Scientific Computing at the University of Southern Denmark, Odense, Denmark. S. Christensen acknowledges financial support from DANISCO A/S. G. H. Peters acknowledges financial support from the Danish National Research Foundation via a grant to MEMPHYS.

References

[1] J.G. Kirkwood, F.P. Buff. The statistical mechanical theory of solutions. i. *J. Chem. Phys.*, **19**(6), 774 (1951).
[2] J.P. O'Connell. Thermodynamic properties of solutions based on correlation functions. *Mol. Phys.*, **20**(1), 27 (1971).
[3] A. Ben-Naim. Inversion of the Kirkwood–Buff theory of solutions: application to the water–ethanol system. *J. Chem. Phys.*, **67**(11), 4884 (1977).
[4] E. Matteoli, L. Lepori. Solute–solute interactions in water. II. an analysis through the Kirkwood–Buff integrals for 14 organic solutes. *J. Chem. Phys.*, **80**(6), 2856 (1984).
[5] R.J. Wooley, J.P. O'Connell. Database of fluctuation thermodynamic properties and molecular correlation function integrals for a variety of binary liquids. *Fluid Phase Equilib.*, **66**(3), 233 (1991).

[6] S. Weerasinghe, P.E. Smith. Kirkwood–Buff derived force field for mixtures of acetone and water. *J. Chem. Phys.*, **118**(23), 10663 (2003).
[7] Y.P. Handa, G.C. Benson. Volume changes on mixing two liquids: a review of the experimental techniques and the literature data. *Fluid Phase Equilib.*, **3**(2–3), 185 (1979).
[8] Y.H. Huang, J.P. O'Connell. Corresponding states correlation for the volumetric properties of compressed liquids and liquid mixtures. *Fluid Phase Equilib.*, **37**, 75 (1987).
[9] M.M. Abbott, H.C. van Ness. Vapor–liquid equilibrium: part 3. Data reduction with precise expressions for g^e. *AIChE J.*, **21**(1), 62 (1975).
[10] I. Nagata, T. Ohta, T. Takahashi, K. Gotoh. Thermodynamic properties of methyl acetate–benzene and methyl acetate–cyclohexane mixtures. *J. Chem. Eng. Jpn.*, **6**, 129 (1973).
[11] E. Matteoli, G.A. Mansoori. *Fluctuation Theory of Mixtures, Advances in Thermodynamics*, Volume 2. Taylor and Francis, New York (1990).
[12] L. Kalé, R. Skeel, M. Bhandarkar, R. Brunner, A. Gursoy, N. Krawetz, J. Phillips, A. Shinozaki, K. Varadarajan, K. Schulten. Namd2: Greater scalability for parallel molecular dynamics. *J. Comp. Phys.*, **151**(1), 283 (1999).
[13] A.D. MacKerell Jr., D. Bashford, M. Bellott Jr., R.L. Dunbrack, J.D. Evanseck, M.J. Field, S. Fischer, J. Gao, H. Guo, S. Ha, D. Joseph-McCarthy, L. Kuchnir, K. Kuczera, F.T.K. Lau, C. Mattos, S. Michnick, T. Ngo, D.T. Nguyen, B. Prodhom, W.E. Reiher III, B. Roux, M. Schlenkrich, J.C. Smith, R. Stote, J. Straub, M. Watanabe, J. Wio'rkiewicz-Kuczera, D. Yin, M. Karplus. All-atom empirical potential for molecular modeling and dynamics studies of proteins. *J. Phys. Chem. B*, **102**, 3586 (1998).
[14] A.D. MacKerell Jr., N.K. Banavali. All-atom empirical force field for nucleic acids: II. Application to molecular dynamics simulations of dna and rna in solution. *J. Comp. Chem.*, **21**(2), 105 (2000).
[15] N. Foloppe, A.D. Mackerell. All-atom empirical force field for nucleic acids. I. Parameter optimization based on small molecule and condensed phase macromolecular target data. *J. Comp. Chem.*, **21**(2), 86 (2000).